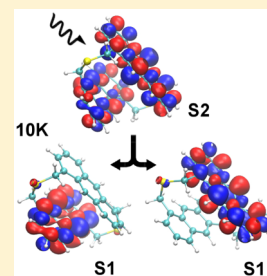


## Photoexcited Energy Transfer in a Weakly Coupled Dimer

Laura Alfonso Hernandez,<sup>†</sup> Tammie Nelson,<sup>‡</sup> Sergei Tretiak,<sup>\*,‡</sup> and Sebastian Fernandez-Alberti<sup>\*,†</sup><sup>†</sup>Universidad Nacional de Quilmes, Roque Saenz Peña 352, B1876BXD Bernal, Argentina<sup>‡</sup>Theoretical Division, Los Alamos National Laboratory, Los Alamos, New Mexico 87545, United States

## Supporting Information

**ABSTRACT:** Nonadiabatic excited-state molecular dynamics (NA-ESMD) simulations have been performed in order to study the time-dependent exciton localization during energy transfer between two chromophore units of the weakly coupled anthracene dimer dithia-anthracenophane (DTA). Simulations are done at both low temperature (10 K) and room temperature (300 K). The initial photoexcitation creates an exciton which is primarily localized on a single monomer unit. Subsequently, the exciton experiences an ultrafast energy transfer becoming localized on either one monomer unit or the other, whereas delocalization between both monomers never occurs. In half of the trajectories, the electronic transition density becomes completely localized on the same monomer as the initial excitation, while in the other half, it becomes completely localized on the opposite monomer. In this article, we present an analysis of the energy transfer dynamics and the effect of thermally induced geometry distortions on the exciton localization. Finally, simulated fluorescence anisotropy decay curves for both DTA and the monomer unit dimethyl anthracene (DMA) are compared. Our analysis reveals that changes in the transition density localization caused by energy transfer between two monomers in DTA is not the only source of depolarization and exciton relaxation within a single DTA monomer unit can also cause reorientation of the transition dipole.



## INTRODUCTION

Exciton transport and (de)localization in extended polymer systems is an important phenomena in photophysics, which impacts optical and electronic properties and the performance of nanophotonic devices such as semiconductor laser diodes,<sup>1</sup> nanowires,<sup>2,3</sup> and photovoltaics,<sup>4</sup> to name a few. From a device design perspective, it is critical to understand how (de)localized states arise in molecular systems and what processes lead to their formation. The intra- and intermolecular energy transfer occurring after photoexcitation and leading to localization or delocalization can have a profound effect on achieving the final desired properties of a device. For example, formation of delocalized excimer states due to interchain aggregation in conjugated polymer-based films has been shown to cause low-energy emission and reduced stability,<sup>5,6</sup> which is undesirable for application in light-emitting devices. In polyfluorenes, stabilization of the light-emission can be achieved through localization of the final fluorescent state on a single chain. A recent theoretical study has demonstrated that this could be achieved using spiro-linked conjugated polyfluorene that prevent  $\pi$ -stacking.<sup>7</sup> In photovoltaics, it has been well-known that the efficiency of charge separation and photocurrent yield in polymer semiconductors depends on the localization of electron and hole states. For example, in MEH-PPV, electronic excitation from a delocalized (localized) occupied orbital to a localized (delocalized) unoccupied orbital gives rise to charge transfer states that produce unusually large photocurrents.<sup>4</sup>

Much effort has been devoted to understanding the highly efficient coherent exciton transport observed in naturally occurring complexes, such as light harvesting systems, in hopes of replicating their efficient energy transfer properties in tailor-made organic semiconductors for technological applica-

tions.<sup>8–12</sup> Furthermore, branched dendrimers containing intramolecular charge transfer interactions between chromophore units have been shown to produce delocalized excitations upon absorption while the emission always occurs from a state localized on a single branch. Indeed, this phenomena of excitation localization is a general characteristic of branched systems, a finding which can be attributed to coherent coupling between chromophores based on the enhancement of optical properties, such as two-photon absorption.<sup>13,14</sup> However, in so-called push–pull chromophores, single molecule spectroscopy experiments resulted in fluorescence from a delocalized state in contradiction with ensemble measurements.<sup>15</sup>

Bichromophoric compounds containing two identical chromophores have become popular systems, in which to study energy transfer both theoretically and experimentally.<sup>16–20</sup> For example, excitation recurrence between chromophores has been identified as the source of the damped oscillations observed in the anisotropy decay of 2,2'-binaphthyl.<sup>17</sup> Similar studies of energy transfer have recently been performed for dithia-anthracenophane (DTA). Oscillations in time-dependent fluorescence anisotropy measurements of DTA have been attributed to long-lived coherent energy transfer between the monomers<sup>16</sup> and those findings have been supported by recent coherent control fluorescence interference experiments.<sup>18</sup> Furthermore, in an extensive theoretical study, Yang et al.<sup>20</sup> have demonstrated that electronic states in DTA

**Special Issue:** John R. Miller and Marshall D. Newton Festschrift

**Received:** October 20, 2014

**Revised:** December 17, 2014

**Published:** December 19, 2014

can be described as localized Frenkel-type excitons. Using coherent resonance energy transfer (CRET) theory, they have shown that the electronic coupling between monomer units in DTA is significantly weakened by the strong electron–phonon coupling such that the effective coupling is small enough to be consistent with coherent energy transfer dynamics.<sup>20</sup>

In this paper, we use nonadiabatic excited state molecular dynamics (NA-ESMD) simulations to study the photoinduced energy transfer dynamics in the weakly coupled anthracene dimer dithia-anthracenophane (DTA) shown in Figure 1. The

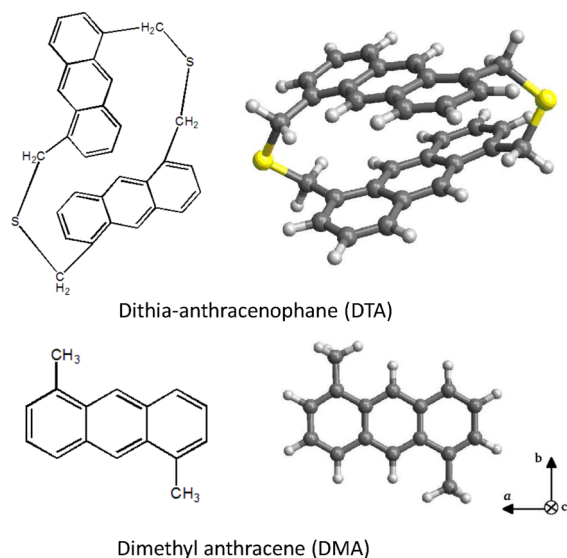


**Figure 1.** Chemical structures and optimized ground state geometries of the dithia-anthracenophane (DTA) bichromophore and its monomer unit, dimethyl anthracene (DMA).

NA-ESMD approach provides a unique advantage of allowing both ensemble and single molecule behavior to be monitored simultaneously. Indeed, we find that at the single molecule level, excitations in DTA are rarely delocalized between the two

anthracene units. Finally, from our simulations we construct simulated fluorescence anisotropy curves based on the change in exciton localization during photodynamics. Our analysis of the simulated fluorescence anisotropy signals for both DTA and its monomer unit dimethyl anthracene (DMA; pictured in Figure 1) reveals that the depolarization observed in DTA is not only due to the interaction between chromophores but is also contributed by exciton relaxation within a single chromophore unit.

## THEORETICAL METHODOLOGY

**Computation of Excited States and NA-ESMD Methodology.** Correlated excited states are calculated using the collective electronic oscillator (CEO) approach<sup>21,22</sup> with the configuration interaction singles (CIS) formalism implemented with the semiempirical PM3 Hamiltonian.<sup>23,24</sup> The CEO approach solves the TDHF equation of motion<sup>25</sup> for the single-electron density-matrix<sup>26</sup> of a molecule driven by an external electric field. The semiempirical approximation retains only a few essential two-electron integrals significantly reducing the numerical demand and allowing for treatment of very large molecular systems. As a trade-off, the TDHF and CIS methods cannot accurately describe excited states with significant double excitation character.<sup>27</sup> Nevertheless, the CEO method has been successfully applied to many molecular systems, including organic conjugated materials<sup>21,28–31</sup> and provides an adequate description of excitonic states and nonadiabatic dynamics in this class of molecular materials.<sup>32</sup>

The NA-ESMD framework provides an efficient and sufficiently accurate method for the simulation of photoinduced dynamics in large molecular systems on picosecond timescales. This is achieved using the fewest switches surface hopping (FSSH) algorithm<sup>33</sup> to allow transitions among coupled electronic states. In this mixed quantum classical approach, the classically treated nuclei evolve on a single adiabatic excited state PES at any given time, and hops from one excited state to another can occur based on the nonadiabatic coupling strengths and a stochastic switching routine.<sup>34</sup> Here, the nuclei are

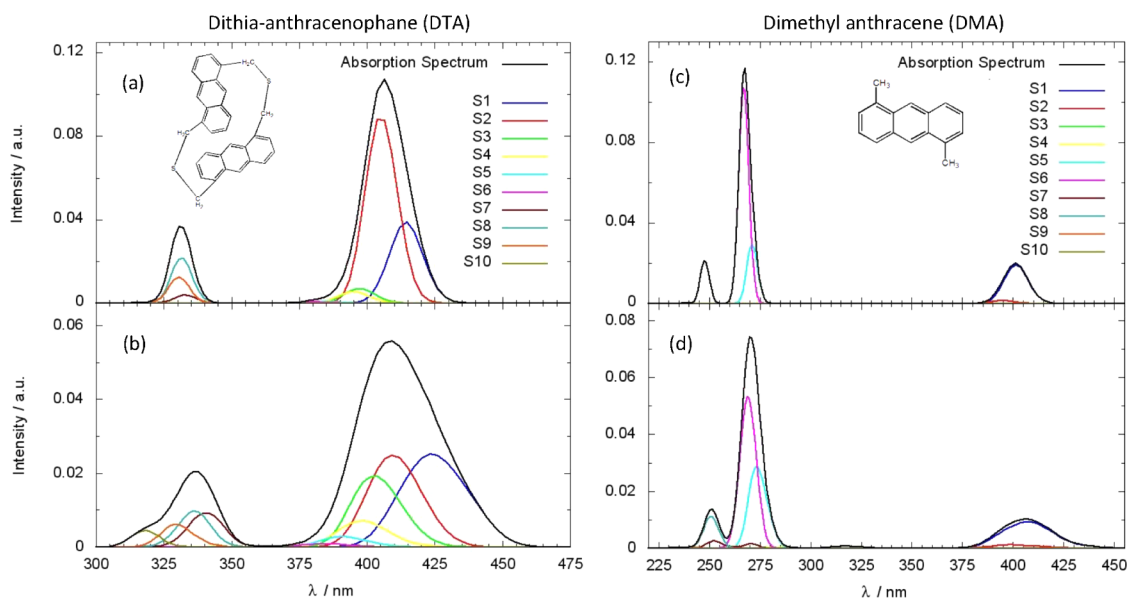


**Figure 2.** Computed absorption spectra where contributions from the 10 lowest energy excited states have been included for the DTA bichromophore at (a) 10 and (b) 300 K and the DMA monomer at (c) 10 and (d) 300 K.

propagated according to a constant-temperature Langevin dynamics algorithm developed to be consistent with the velocity Verlet integration technique.<sup>35</sup> This approach allows for a phenomenological description of solvent effects from frictional damping and the fluctuating force following the fluctuation–dissipation theorem.<sup>36</sup> Meanwhile, electrons have a quantum mechanical description related to excited state energies, gradients, and nonadiabatic coupling terms which are computed “on the fly” with analytical techniques.<sup>37–42</sup> Further details of the NA-ESMD approach, implementation, and limitations can be found in our previous work.<sup>40,43–47</sup>

**Simulation Details and Absorbance Spectra.** We have modeled the photoinduced dynamics of the bichromophore DTA whose chemical structure and optimized ground state (GS) geometry are shown in Figure 1 along with the DMA monomer unit. DTA is a linked bichromophore composed of two anthracene units connected by two thioethers producing a rigid structure with very little conformational flexibility. Both room temperature (300 K) and low temperature (10 K) simulations have been performed. For each temperature, 600 snapshots were collected from thermally equilibrated ground-state MD trajectories (10 and 300 K) propagated using a Langevin thermostat with a friction coefficient of 20 ps<sup>-1</sup>. The snapshots provide initial geometries and momenta for the excited state dynamics. For each initial configuration, oscillator strengths, and energies for the 10 lowest energy excited states were computed and used to construct the linear absorption spectra shown in Figure 2, where the individual contributions of each state are also shown. The spectra are histograms of the excited state energies where the height of the histogram is related to the average ratio between oscillator strength and frequencies<sup>48</sup> for the corresponding state. The spectra for DTA reveal that, at low temperature (10 K; Figure 2a), the peak at 400 nm has dominant contributions from S<sub>2</sub> and S<sub>1</sub>. The peak becomes thermally broadened at room temperature (300 K; Figure 2b) having relatively equal contributions from S<sub>1</sub>–S<sub>3</sub> due to conformational fluctuations and mixing of excited states. In the case of DMA, both the low temperature spectrum (10 K; Figure 2c) and the room temperature spectrum (300 K; Figure 2d) show that the peak near 400 nm is derived only from S<sub>1</sub> corresponding to the single monomer. Less thermal broadening is present in the monomer due to fewer degrees of conformational freedom.

The computed spectra for DTA agree well with previously measured experimental spectra<sup>16</sup> obtained in THF solution, which show four distinct features in the lowest-energy peak between ~350–400 nm. On the basis of the computed spectra, these features correspond to the CIS excitation energies for states S<sub>1</sub>–S<sub>4</sub>, while the peaks below 300 nm in experimental spectra can be assigned to higher lying excited states S<sub>7</sub> and above. In the theoretical work of Yang et al.,<sup>20</sup> the TD-DFT calculations from the optimized ground state geometry resulted in the two lowest energy excited states (S<sub>1</sub> and S<sub>2</sub>) being dark states with no oscillator strength. Thus, they assign the lowest energy peak in the experimental spectra to S<sub>3</sub> and S<sub>4</sub>. Nonetheless, the 408 nm pump pulse previously used in the experiment<sup>16</sup> is then consistent with excitation to either S<sub>1</sub> and S<sub>2</sub> (CIS) or S<sub>3</sub> and S<sub>4</sub> (TD-DFT). Therefore, we have chosen an excitation wavelength to the blue side of the lowest energy peak in the simulated absorption spectra to be consistent with refs 20 and 16, corresponding to S<sub>3</sub> and S<sub>4</sub> CIS states.

A simulated laser pulse is used to populate the initial excited state for each geometry according to a Franck–Condon

window given by  $g_\alpha(\mathbf{r}, \mathbf{R}) = (f_\alpha/\Omega_\alpha^2) \exp[-T^2 (E_{\text{laser}} - \Omega_\alpha)^2]$ .  $f_\alpha$  represents the normalized oscillator strength for state  $\alpha$  whose frequency is given by  $\Omega_\alpha$  and  $E_{\text{laser}}$  represents the energy of a laser centered at 400 nm (300 K) and 396 nm (10 K). A Gaussian laser pulse,  $f(t) = \exp(-t^2/2T^2)$ , with  $T^2 = 42.5$  fs corresponding to a fwhm (full width at half maximum) of 100 fs has been used. Following excitation, 600 NA-ESMD trajectories were propagated using Langevin dynamics for 900 fs with a nuclear time step of 0.1 fs, electronic time step of 0.025 fs, and Langevin friction coefficient of 20 ps<sup>-1</sup>, where 6 lowest energy excited states and their corresponding non-adiabatic coupling vectors have been included in the dynamics. The quantum time step was further reduced by a factor of 40 in order to identify trivial unavoided crossings.<sup>44</sup>

**Transition Density Localization.** The exciton localization can be followed by tracking changes in the spatial localization of the electronic transition density (TD). The CEO approach<sup>21,22</sup> is used to calculate transition density matrices

$$(\rho^{0\alpha})_{nm} = \langle \phi_\alpha(r; \mathbf{R}(t)) | c_m^+ c_n | \phi_0(r; \mathbf{R}(t)) \rangle \quad (1)$$

where the CIS adiabatic ground and excited state wave functions are represented by  $\phi_0(r; \mathbf{R}(t))$  and  $\phi_\alpha(r; \mathbf{R}(t))$ , respectively.  $n$  and  $m$  are indices referring to the atomic orbital (AO) basis functions and  $c_m^+$  and  $c_n$  are creation and annihilation operators such that the diagonal elements  $(\rho^{0\alpha})_{nn}$  represent the net change in the electronic density distribution caused by excitation from the ground state S<sub>0</sub> to an excited electronic state S <sub>$\alpha$</sub> .<sup>49</sup> The usual normalization condition  $\sum_{n,m} (\rho^{0\alpha})_{nm}^2 = 1$  holds for the CIS approximation.<sup>37</sup> The fraction of the transition density localized on each anthracene unit is obtained by summing the contributions from each atom (index A) as follows

$$(\rho^{0\alpha})_{X\text{-unit}}^2 = \sum_{n_A m_A} (\rho^{0\alpha})_{n_A m_A}^2 \quad (2)$$

In this way, TD analysis provides a simplified picture of wave function dynamics that do not depend on the population of adiabatic states.

## RESULTS AND DISCUSSION

**Initial Localization.** At the GS minimum, excitonic coupling between the chromophore units induces delocalization and the four lowest energy excited states S<sub>1</sub>–S<sub>4</sub> are completely delocalized between both anthracene units as can be seen from the electronic transition densities shown in Figure S1 (see the Supporting Information). This coupling (and the Davydov splitting between pairs of states) is small. Davydov splitting in singlet exciton states of crystalline anthracene and pentacene is well-known.<sup>50–52</sup> Therefore, the delocalization may not persist during equilibrated GS dynamics due to thermal fluctuations that break the dimer symmetry and overcome electronic communications. Thus, the excited states evaluated at the initial configurations used in NA-ESMD differ from those shown in Figure S1 of the Supporting Information. The linear combination of a localized anthracene monomer excited state produces two dimer states where the symmetric (delocalized) component is at a higher energy than the antisymmetric (localized) component. Using the anthracene unit with the larger initial fraction of S<sub>1</sub> transition density [ $(\rho^{01})_{\text{monomer}}^2 > 0.5$  at  $t = 0$  fs] as a reference, we have analyzed the fraction of the transition density of the other states (S<sub>2</sub>–S<sub>4</sub>) by constructing histograms of the transition density for all

initial configurations. The analysis at 300 K, shown in Figure 3a, reveals that  $S_1$  is strongly localized in one monomer and  $S_3$  is

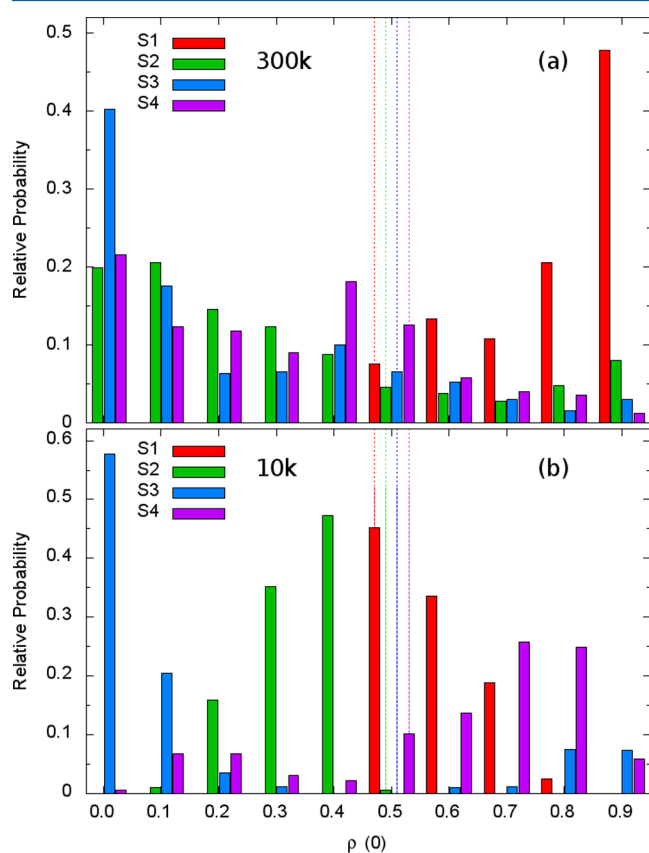


**Figure 3.** Distribution over all initial configurations at (a) 300 and (b) 10 K of the transition density of the 4 lowest energy excited states in the monomer where  $S_1$  is initially localized [ $(\rho^{01})^2_{\text{monomer}} > 0.5$  at  $t = 0$  fs]. The dashed lines correspond to the equilibrium geometry.

mainly localized in the other monomer, while  $S_2$  and  $S_4$  are more delocalized. Therefore, the geometry distortions introduced by temperature (300 K) break the symmetry and destroy the complete delocalization of the equilibrium geometry observed in Figure S1 of the Supporting Information (equilibrium values are indicated by dashed lines in Figure 3).  $S_1$  and  $S_3$  dimer excitations correspond to the antisymmetric (localized) Davydov component of  $S_1$  and  $S_2$  monomer states, respectively, and are localized on different units of the dimer. Similarly,  $S_2$  and  $S_4$  dimer states arise from the symmetric (delocalized) combinations of monomer states. The corresponding TD distribution at 10 K is shown in Figure 3b. At low temperature,  $S_1$  and  $S_2$  remain delocalized since the conformational deformations from the well-delocalized GS equilibrium structure are not sufficiently large to induce localization. On the contrary,  $S_3$  is completely localized while  $S_4$  is only partially localized, suggesting that  $S_3$  and  $S_4$  states are more susceptible to thermal fluctuations.

It is important to note that, during dynamics, no significant changes in the distance or relative orientation between the anthracene units are observed. To verify this, we have identified three parameters to monitor: the distance between the center of mass of each monomer, the angle between the planes containing each monomer (each plane defined by three benzene rings), and the angle between the main inertial axis of each monomer. Histograms of the monitored distance and

angles during equilibrated GS dynamics at 300 K can be seen in Figure S2 (panels a–c) (see the Supporting Information). These motions correspond to geometrical distortions due to thermal fluctuations at the GS that define the initial conditions for NA-ESMD simulations. The center of mass distance (Figure S2a of the Supporting Information) displays minor variations having an average value of  $3.67 \pm 0.16$  Å. The average angle between the planes formed by each anthracene unit (Figure S2b of the Supporting Information) is  $8.40 \pm 5.05^\circ$ , indicating that the units remain relatively parallel to each other. Finally, the average angle between the inertial axis of each anthracene unit (Figure S2c of the Supporting Information) has a value of  $89.98 \pm 0.12^\circ$ . Naturally, even less variation in the distances and angles is expected at low temperature where thermally induced fluctuations are smaller. Therefore, no significant molecular distortions occur during dynamics.

However, within the relevant range experienced during dynamics, geometry distortions are responsible for the thermally induced localization of states that are previously delocalized at the GS minimum. As can be seen in Figure S3 (see the Supporting Information), starting from the equilibrium GS geometry, distortions along the center of mass coordinate and the angle between the anthracene planes causes the transition density of the four lowest energy excited states to experience regions of configuration space where strong localization occurs, consistent with the localization observed in the ensemble at room temperature (Figure 3a). These coordinates involve collective relative displacements between the anthracene units and are thus expected to be related to low-frequency normal modes of the dimer. The zero-point energy varies linearly with mode frequency leading to low values of zero-point energies for these collective motions and therefore, no significant effects on our findings. Furthermore, these plots confirm that the  $S_3$  and  $S_4$  states are more strongly affected by small geometry distortions, leading to localization of  $S_3$  and, to a lesser extent  $S_4$ , even at low temperature as observed in Figure 3b. The variation of the angle between the main inertial axis of each monomer did not produce changes in the localization.

**Photoinduced Exciton Redistribution.** The evolution of the average transition density localized in each anthracene unit provides a picture of the exciton dynamics of the ensemble. In order to analyze this, we differentiate the anthracene units based on the transition density localization of the initial excited state denoted  $i$ : monomer A is assigned as the anthracene unit with the larger initial fraction of transition density ( $(\rho^{0i})^2_A > 0.5$  at  $t = 0$  fs), and monomer B is the other such that the initial excitation is always primarily localized in monomer A. Figure 4 (panels a and b) shows the time dependence of the average fraction of transition density localized in monomers A (black line) and B (red line) during simulations at 10 and 300 K, respectively, averaged over the ensemble of trajectories. At both temperatures, the decay of the transition density of monomer A is concomitant with the rise in the transition density of monomer B, such that both arrive at 50% within 10 fs. Since this is an ensemble average, it does not reveal the actual distribution (or the actual underlying composition of the distribution) of the exciton localization. Instead, Figure 4 (panels a and b) reveals that within 10 fs, monomers A and B are no longer distinguishable as the average fraction of transition density in each unit becomes more or less equivalent on a very fast timescale.

To demonstrate this point, the reader can imagine two scenarios: (1) In all trajectories, each of the anthracene units

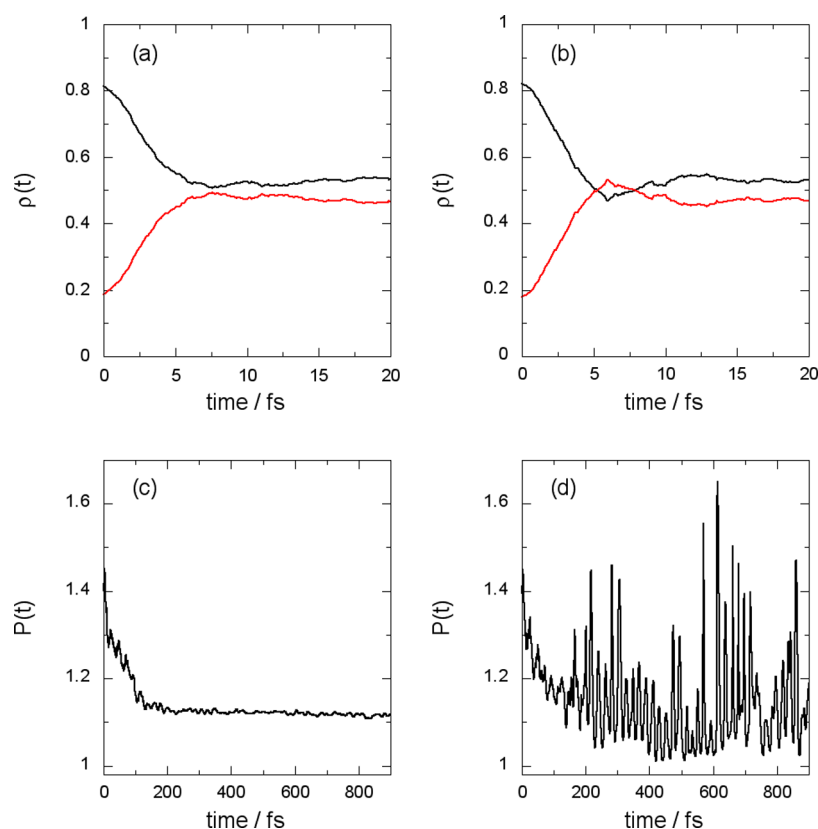


**Figure 4.** Time dependence of the average fraction of TD localized on the monomer (A) where  $S_1$  is initially localized [ $(\rho^{0i})_A^2 > 0.5$  at  $t = 0$  fs] (black line), and the other monomer (B) (red line) is plotted at (a) 10 and (b) 300 K. Participation number (defined taking the monomers as units) is at (c) 10 and (d) 300 K.

receives half of the transition density. (2) In half of the trajectories, the transition density becomes completely localized in the initially excited monomer (monomer A), and in the other half of trajectories, the transition density is completely localized in monomer B. In the first scenario, the excitation is delocalized between both anthracene units, while in the second example, the excitation is localized in either one monomer or the other with equal probability. However, in the ensemble average, each monomer would have 50% of the average transition density as seen in Figure 4 (panels a and b).

Therefore, we cannot determine from Figure 4 (panels a and b) alone whether localization (and thus energy transfer) occurs. Instead, the analysis of the participation number is used. The extent of (de)localization of the excitation can be seen from the participation number given by

$$P = \left[ \sum_X ((\rho^{0\alpha})_{X\text{-unit}}^2)^{-1} \right] \quad (3)$$

where  $X = A$  and  $B$ . The participation number is defined taking each monomer as a unit such that  $1 \leq P \leq 2$ . Therefore,  $P \approx 1$  corresponds to complete localization of the transition density to a single anthracene unit and  $P \approx 2$  represents delocalization of the transition density over both units. The evolution of the participation number during the NA-ESMD simulations at 10 and 300 K is plotted in Figure 4 (panels c and d, respectively). At low temperature, it is clear that the dynamics leads to a localization of the transition density to a single anthracene unit within 200 fs seen by the decay of the participation number from an initial value of  $P \approx 1.5$  to  $P \approx 1.1$ . At 300 K, a mixture of localized and delocalized excitations persists throughout the

dynamics. Therefore, the evolution of the participation numbers (Figure 4, panels c and d) suggests that fast localization to a single monomer unit indeed occurs.

In order to understand whether this localization is a result of energy transfer, we have classified the trajectories according to the relative localization of the final transition density ( $t = 900$  fs) with respect to its initial localization ( $t = 0$  fs). Accordingly, there are two types of trajectories: those whose final transition density is primarily localized on the same monomer as the initial transition density (type I), and those whose final transition density is primarily localized in the monomer that initially had less transition density (type II). That is, type II trajectories correspond to trajectories that follow pathways that lead to an effective intermonomer energy transfer at long times. Both types I and II initially have 80% transition density localized in monomer A. However, type I remains localized in the same monomer, while type II switches its localization to monomer B. We find that there are 266 type I trajectories and 223 type II trajectories at 10 K and 158 type I trajectories and 171 type II trajectories at 300 K such that nearly half of the trajectories finish with the transition density completely localized in the initially excited monomer, while the other half of the trajectories finish with the transition density completely localized in the opposite monomer, as in scenario (2) described above.

These two types can be seen in Figure 5. These 3D histograms follow the time-evolution of the transition density localized in the monomer that initially had the larger transition density (monomer A) for types I (red) and II (blue) trajectories at 10 and 300 K. At 10 K, the histogram for type

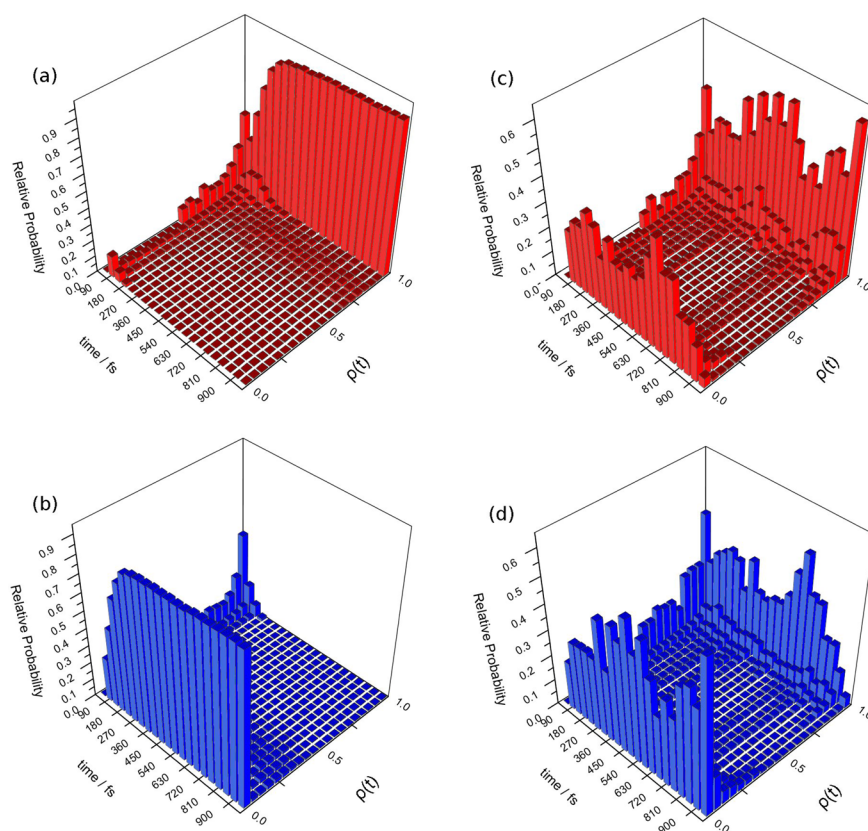


**Figure 5.** Time-dependent histograms of the transition density evolution. Each histogram plots the fraction of the TD localized on the monomer with the larger initial TD for (a) type I trajectories at 10 K; (b) type II trajectories at 10 K; (c) type I trajectories at 300 K; and (d) type II trajectories at 300 K.

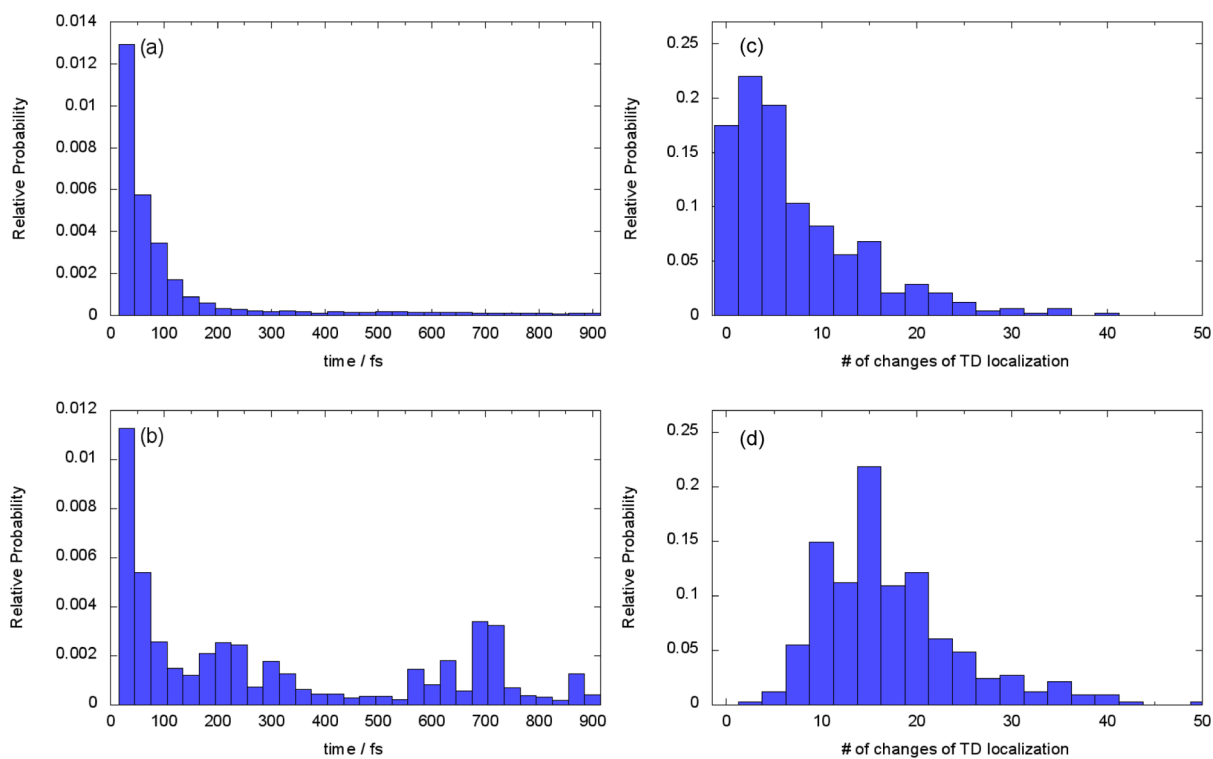


**Figure 6.** Relative probability of changing the TD localization as a function of time at (a) 10 and (b) 300 K. Histogram of the number of times the TD localization changes between the monomers during dynamics at (c) 10 and (d) 300 K.

I (Figure 5a) confirms that the excitation in these trajectories remains strongly localized on the same anthracene unit throughout the dynamics with no probability of having localization less than  $\approx 0.8$ . The initial excitation has a small probability of being delocalized, but it quickly localizes with highest probability  $\delta \approx 1.0$ . A small probability of being localized on the opposite anthracene monomer exists only at short times, while the probability of being delocalized ( $0.3 \leq \delta \leq 0.7$ ) becomes virtually negligible even at short times. In an equivalent way, the excitation for type II trajectories (Figure 5b) is initially localized primarily on one anthracene unit with small probability of delocalization. Nevertheless, at short times ( $\approx 200$  fs), the excitation becomes completely localized on the opposite anthracene unit. Following localization, the exciton relaxation occurs only in one monomer.

The evolution of the transition density localization at room temperature (300 K) for types I (Figure 5c) and II (Figure 5d) trajectories reveals clear differences from the low-temperature result. Here there are continuous changes in the localization throughout the simulation. While Figure 4 (panels a and b) seems to indicate that the dynamics at 10 K are similar to 300 K, this is not true. In both cases, half of the trajectories finish with the exciton localized in the initially excited monomer, and the other half of the trajectories finish with the exciton localized on the other monomer. At 10 K, this is due to an ultrafast initial transfer due to a transient delocalization that is not observed at longer times. However, at 300 K, a constant transfer of the exciton from one monomer to the other is observed, where the exciton is localized in one anthracene unit or the other but rarely delocalized between both.

The changes in localization can be seen more clearly in Figure 6. The relative probability that a trajectory will experience a change in TD localization at any given time during dynamics is shown in Figure 6 (panels a and b). As can be seen, at 10 K (Figure 6a), most transitions take place before 200 fs, indicating that the complete relaxation of the exciton generally takes place on one monomer after the changes in localization have already occurred. Meanwhile, the changes in localization persist throughout the dynamics at 300 K (Figure 6b). Not only do the changes in TD localization occur at different times for 10 and 300 K, there is also a difference in the absolute number of changes in TD localization. For a given trajectory, the average number of changes in TD localization between the monomers is shown in Figure 6 (panels c and d). For a trajectory at 10 K (Figure 6c), the average number of changes in TD localization is 1–2, which is significantly lower than for 300 K (Figure 6d), where a trajectory will experience a change in TD localization an average of 14 times. The increased changes in TD localization at 300 K is a result of temperature-induced geometry distortions that change the TD localization. However, the changes at 10 K are not limited to just 1 or 2, as could be expected from Figures 5 (panels a and b) and 6a. Analyzing the individual trajectories, we have observed that occasionally at 10 K, the complete relaxation of the exciton in one monomer does not occur, but it is still a less frequent event compared to 300 K.

Previous analysis of energy transfer dynamics in DTA in terms of CRET theory<sup>20</sup> showed an oscillatory behavior in the donor population with a 1.2 ps period matching the experimentally observed oscillations in fluorescence anisotropy measurements.<sup>16</sup> This energy transfer recurrence is clearly observed in our simulations as the exciton localized on one monomer or the other hops back and forth between the two

chromophores, suggesting wavelike energy transfer dynamics. Along these lines, Figure 6 (panels a and b) can be interpreted as the relative probability of energy transfer recurrence. At low temperature, the oscillations in donor population become quickly damped. However, at 300 K, the initial damping is fast and followed by persistent hops due to thermal fluctuations which can change the dynamics to incoherent resonance energy transfer. In order to compare with previous studies, it is important to note that experimental data has been obtained in THF solution. Therefore, the Coulombic interaction between chromophores in our simulations should be screened by a factor of  $n^2 = 1.98$ . From the dynamics at 10 K, we can make a rough estimate of the oscillation period: from Figure 6a, it is clear that the majority of transitions take place within the first 200 fs where there are an average of 1–2 hops (200–400 fs period). Combined with the simple screening correction, this gives an oscillation period of 0.8–1.6 ps, in good agreement with the reported value of 1.2 ps.

**Fluorescence Anisotropy Decay.** The time-resolved fluorescence anisotropy can be used to follow changes in the exciton localization during photodynamics. The fluorescence anisotropy is calculated using the autocorrelation function of the absorption dipole moment of the fluorophore at time zero,  $\vec{\mu}_A(t=0)$ , and its emission dipole moment at time  $t$ ,  $\vec{\mu}_E(t)$ ,<sup>53</sup> according to the following

$$r(t) = \frac{2}{5} \langle P_2\{\vec{\mu}_A(0) \cdot \vec{\mu}_E(t)\} \rangle \quad (4)$$

where  $P_2(x) = (1/2)(3x^2 - 1)$  is the second-order Legendre polynomial, and the angular brackets indicate the average over all of the trajectories.

The resulting fluorescence anisotropy curves are plotted in Figure 7 at 300 K for DTA (black line) as well as the monomer

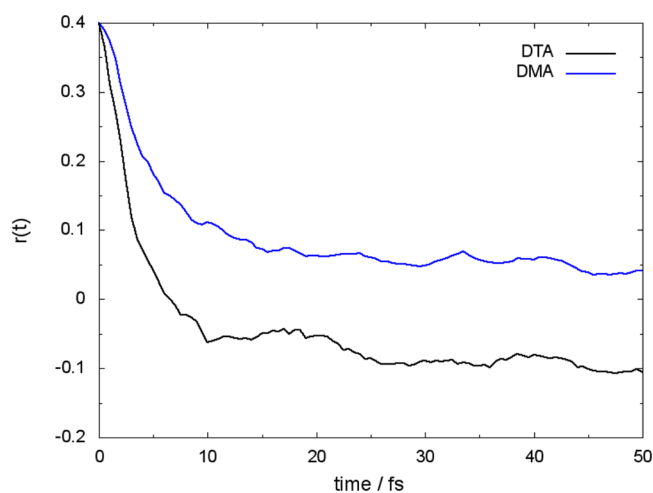


**Figure 7.** Simulated fluorescence anisotropy decay at 300 K for DMA (blue line) and DTA (black line).

DMA (blue line). The rigid structure of the DTA dimer results in a relatively long dephasing time (1 ps).<sup>20</sup> Compared to the much slower 30 ps time constant for rotational diffusion,<sup>16</sup> the energy transfer dynamics essentially occur at a fixed orientation without the effect of rotational motion on the anisotropy. Therefore, we can safely assume that the energy transfer between monomers is the only source of fluorescence depolarization and rotational diffusion can be neglected. The decay observed for DTA is not only due to the change of

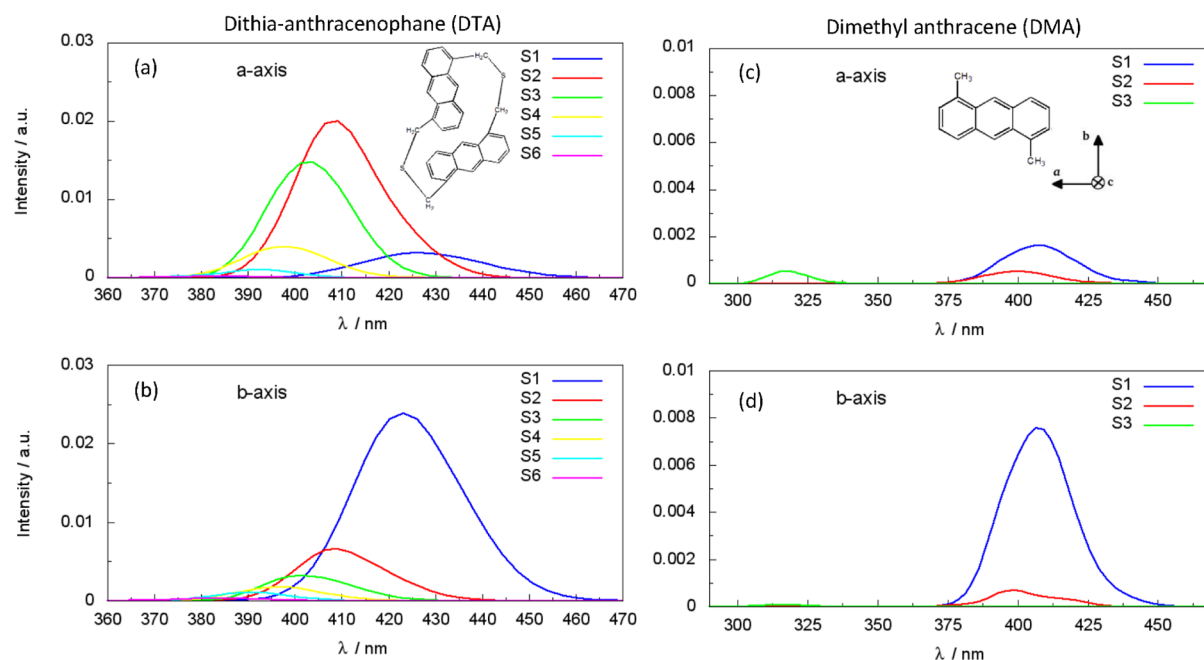


**Figure 8.** Polarized absorption spectra computed at 300 K, where individual contributions from each excited state have been included. Absorption is polarized along the principal inertial monomer axis along the backbone (*a* axis) and the perpendicular bisecting axis (*b* axis) for DTA (a) *a* and (b) *b* axes. Corresponding spectra for DMA (c) *a* and (d) *b* axes.

localization of the exciton between both monomers, but the relaxation within a unique monomer also leads to a change in the orientation of the emission dipole moment. This can be seen from the fluorescence anisotropy for DMA where exciton relaxation is necessarily confined to the single monomer. In that case, fluorescence depolarization associated with the relaxation on a single monomer is observed.

By definition, the anisotropy  $r(t)$  must be within the range from  $-0.20$  to  $0.40$  for single-photon excitation.<sup>54</sup> The initial value  $r(0) = 0.4$  corresponds to an angle of  $0^\circ$  between the absorption and emission dipoles. In DMA, a value close to  $0.1$  is reached corresponding to an angular displacement of  $45^\circ$  between transition dipole moments on a single monomer. Negative values of  $r(t)$  observed in DTA correspond to angular displacements between the monomers, ranging from  $54.7^\circ$  at  $r(t) = 0$  and  $90^\circ$  for  $r(t) = -0.20$ . The additional depolarization below  $r(t) \approx 0.1$  in DTA compared to DMA is a result of the change in TD localization between rotated monomers due to energy transfer.

To verify this, we have computed polarized absorption spectra, provided in Figure 8, for both DTA and DMA at room temperature (300 K). The monomer DMA has been oriented in the direction of the principal inertial axis. For DTA, rather than choosing the principal inertial axis of the entire dimer, we have chosen the principal axis of the monomer with the larger initial transition density. For this analysis, each initial ground state configuration has been translated to a body fixed reference frame with its origin at the corresponding center of mass. Then, the mutually orthogonal principal axes of rotation (*a*, *b*, and *c*) of the rigid body are obtained from the eigenvectors of the moment of inertia tensor. The first moment of inertia, *a*, is oriented mainly along the long axis of the monomer unit, and the molecular plane corresponds to the plane formed by the *a* and *b* axes. As an example, Figure 1 displays the PM3 optimized structure of DMA oriented along its principal inertial axes. The Cartesian coordinate axes of each ground-state configuration

are reoriented so they coincide with their corresponding principal axes of rotation, and the transition dipole moments are then calculated within this new body fixed reference frame. The spectra have been computed according to the procedure outlined in Theoretical Methodology where the individual contributions from the 6 lowest energy excited states have been included for DTA, and the 3 lowest energy excited states are included for DMA.

As can be seen, the absorption of the  $S_1$  state in DTA is mainly in the direction of the *b* axis (Figure 8b), and the same can be observed in DMA (Figure 8d). Since, by our selection of the body fixed reference frame,  $S_1$  is strongly localized in the monomer aligned with the backbone perpendicular to the *b* axis for DTA, absorption in the *b* axis indicates localization to the aligned monomer, in agreement with the polarized absorption observed in DMA. Recall that the average angle between the inertial axes of the monomers in DTA at room temperature is close to  $90^\circ$  (Figure S2c of the Supporting Information), so that the *b* axis of one monomer corresponds to the *a* axis of the other. Therefore, if the state is delocalized, absorption will be mixed in both directions. In the case of  $S_2$ , which is quite delocalized between monomers but is mainly in another monomer with respect to  $S_1$  (Figure 3a), absorption is primarily in the *a* axis and less in the *b* axis direction (Figure 8, panels a and b). Something similar happens with  $S_3$ : this state is more localized than  $S_2$ , though still primarily localized in the opposite monomer with respect to  $S_1$  (Figure 3a). As can be seen in Figure 8 (panels a and b),  $S_3$  absorption in DTA is primarily in the *a* axis direction and is less mixed with absorption in the *b* axis compared to the more delocalized  $S_2$  state.

In DMA, the relaxation occurs in the single monomer. In this case,  $S_3$  absorbs primarily in the *a* axis,  $S_2$  is somehow mixed, and  $S_1$  absorbs mainly in the *b* axis. This changing polarization during relaxation results in the fluorescence anisotropy decay observed in Figure 7. The same effect occurs in DTA, where states  $S_2$  and higher are mixed and absorb primarily in the *a* axis

while  $S_1$  absorbs in the  $b$  axis. Relaxation on a single monomer in DTA would still lead to fluorescence anisotropy decay due to this difference of polarization and mixing among the excited states. During energy transfer between monomers in DTA, the  $a$  and  $b$  axes become somehow inverted, depending on the angular displacement between the monomers. The additional depolarization seen in Figure 7 for DTA is caused by this polarization inversion due to energy transfer between the rotated monomers.

## CONCLUSION

We have performed NA-ESMD simulations of the bichromophore DTA at both low temperature (10 K) and room temperature (300 K) to study the exciton (de)localization between two chromophore units during energy transfer. The energy transfer pathways between anthracene units persist at low temperature due to the initially strong nonadiabatic coupling between states that leads to an ultrafast exchange of energy between monomers. In both low and room temperature cases, thermal fluctuations break the delocalization of the optimized ground state geometry and lead to localized exciton states. During dynamics, half of the trajectories finish completely localized on the same monomer on which the initial excitation was localized, and half of them become completely localized on the other monomer without ever being delocalized between them. At 10 K, relatively few changes in TD localization (1 or 2) occur within the first 200 fs of dynamics followed by the complete exciton relaxation on only one monomer. At 300 K, many changes in TD localization ( $\sim 14$ ) persist throughout the entire dynamics due to thermally induced geometric distortions which bring electronic states into resonance. Because of the resonant energy transfer, we have observed that the complete relaxation within a single monomer is less frequent at 300 K, although not absent, as the hopping between chromophores continues for long times.

We observe that the time at which the molecular system reaches an equal distribution of localized transition density among the two chromophore units is temperature-independent. Nevertheless, while at 10 K, the exciton gets trapped in a unique anthracene unit during the first 200 fs, energy transfer events persist at 300 K for longer times. We can attribute this latter behavior to the observed high sensitivity of the transition density localization to relatively small geometry distortions introduced by thermal fluctuations. Furthermore, we have verified that at both room temperature and low temperature, the DTA molecule never becomes trapped in any long-lived transient excited state during photodynamics where the transition density would be delocalized among the two anthracene units.

Simulated fluorescence anisotropy curves have been computed from the dipole moment autocorrelation function for both the bichromophore DTA and its monomer DMA at room temperature. The anisotropy signal of DMA essentially reveals the extent of depolarization due to exciton relaxation within a single monomer. The additional depolarization in DTA results from changes in TD localization between rotated monomer units. However, that is not the only source of fluorescence anisotropy in the bichromophore system since the relaxation within a unique monomer also leads to a change in the orientation of the absorption dipole moment as observed in DMA.

## ASSOCIATED CONTENT

### Supporting Information

Electronic transition density localization at the ground state minimum, distribution of molecular configurations during ground state dynamics, and geometry induced variations of transition density localizations. This material is available free of charge via the Internet at <http://pubs.acs.org>.

## AUTHOR INFORMATION

### Corresponding Authors

\*E-mail: [serg@lanl.gov](mailto:serg@lanl.gov).

\*E-mail: [sfalberti@gmail.com](mailto:sfalberti@gmail.com).

### Notes

The authors declare no competing financial interest.

## ACKNOWLEDGMENTS

L.A.H. and S.F.A. are supported by CONICET, UNQ, ANPCyT (PICT-2010-2375). S.T. and T.N. acknowledge support from Los Alamos National Laboratory (LANL) Directed Research and Development Funds. Los Alamos National Laboratory is operated by Los Alamos National Security, LLC, for the National Nuclear Security Administration of the U.S. Department of Energy under contract DE-AC52-06NA25396. We acknowledge support of the Center for Integrated Nanotechnology (CINT), a U.S. Department of Energy, Office of Basic Energy Sciences user facility.

## REFERENCES

- (1) Mickevicius, J.; Jurkevicius, J.; Kazlauskas, K.; Zukauskas, A.; Tamulaitis, G.; Shur, M. S.; Shatalov, M.; Yank, J.; Gaska, R. Stimulated Emission Due to Localized and Delocalized Carriers in  $\text{Al}_{0.35}\text{Ga}_{0.65}\text{N}/\text{Al}_{0.49}\text{Ga}_{0.51}\text{N}$  Quantum Wells. *Appl. Phys. Lett.* **2012**, *101*, 041912.
- (2) Voss, T.; Bekeny, C.; Gutowski, J.; Tena-Zaera, R.; Elias, J.; Levy-Clement, C.; Mora-Sero, I.; Bisquert, J. Localized Versus Delocalized States: Photoluminescence From Electrochemically Synthesized ZnO Nanowires. *J. Appl. Phys.* **2009**, *106*, 054304.
- (3) Koch, M.; Ample, F.; Joachim, C.; Grill, L. Voltage Dependent Conductance of a Single Graphene Nanoribbon. *Nat. Nanotechnol.* **2012**, *7*, 713–717.
- (4) Kohler, A.; Santos, D. A. D.; Beljonne, D.; Shuai, Z.; Bredas, J.-L.; Holmes, A. B.; Kraus, A.; Mullen, K.; Friend, R. H. Charge Separation in Localized and Delocalized Electronic States in Polymeric Semiconductors. *Nature* **1998**, *392*, 903–906.
- (5) Nguyen, T.-Q.; Martini, I. B.; Liu, J.; Schwartz, B. J. Controlling Interchain Interactions in Conjugated Polymers: The Effects of Chain Morphology on Exciton-Exciton Annihilation and Aggregation in MEH-PPV Films. *J. Phys. Chem. B* **2000**, *104*, 237–255.
- (6) Sims, K.; Bradley, D.; Ariu, M.; Koeberg, M.; Asimakis, A.; Grell, M.; Lidzey, D. G. Understanding the Origin of the 535 nm Emission Band in Oxidized Poly(9,9-dioctylfluorene): The Essential Role of Inter-Chain/Inter-Segment Interactions. *Adv. Funct. Mater.* **2004**, *14*, 765–781.
- (7) Ondarse-Alvarez, D.; Oldani, N.; Tretiak, S.; Fernandez-Alberti, S. *Photoexcited Dynamics in Weakly Interacting Conjugated Molecular Aggregates* **2014**, unpublished.
- (8) Aggarwal, A. V.; Thiessen, A.; Idelson, A.; Kalle, D.; Wursch, D.; Stangl, T.; Steiner, F.; Jester, S.-S.; Vogelsang, J.; Hoger, S.; et al. Fluctuating Exciton Localization in Giant  $\pi$ -Conjugated Spoked Wheel Macrocycles. *Nat. Chem.* **2013**, *5*, 964–970.
- (9) Fernandez-Alberti, S.; Roitberg, A.; Kleiman, V.; Nelson, T.; Tretiak, S. *J. Chem. Phys.* **2012**, *137*, 22A526.
- (10) Ortiz, W.; Krueger, B. P.; Kleiman, V. D.; Krause, J. L.; Roitberg, A. E. Energy Transfer in the Nanostar: The Role of Coulombic Coupling and Dynamics. *J. Phys. Chem. B* **2005**, *109*, 11512–11519.

- (11) Fernandez-Alberti, S.; Kleiman, V. D.; Tretiak, S.; Roitberg, A. E. Nonadiabatic Molecular Dynamics Simulations of the Energy Transfer Between Building Blocks in a Phenylene Ethynylene Dendrimer. *J. Phys. Chem. A* **2009**, *113*, 7535–7542.
- (12) Arias, D. H.; Stone, K. W.; Vlaming, S. M.; Walker, B. J.; Bawendi, M. G.; Silbey, R. J.; Bulovic, V.; Nelson, K. A. Thermally-Limited Exciton Delocalization in Superradiant Molecular Aggregates. *J. Phys. Chem. B* **2013**, *117*, 4553–4559.
- (13) Katan, C.; Terenziani, F.; Mongin, O.; Werts, M. H. V.; Porres, L.; Pons, T.; Mertz, J.; Tretiak, S.; Blanchard-Desce, M. Effects of (Multi)branching of Dipolar Chromophores on Photophysical Properties and Two-Photon Absorption. *J. Phys. Chem. A* **2005**, *109*, 3024–3037.
- (14) Terenziani, F.; Katan, C.; Badaeva, E.; Tretiak, S.; Blanchard-Desce, M. Enhanced Two-Photon Absorption of Organic Chromophores: Theoretical and Experimental Assessments. *Adv. Mater.* **2008**, *20*, 4641–4678.
- (15) Aumiler, D.; Wang, S.; Chen, X.; Xia, A. Excited State Localization and Delocalization of Internal Charge Transfer in Branched Push-Pull Chromophores Studied by Single Molecule Spectroscopy. *J. Am. Chem. Soc.* **2009**, *131*, 5742–5743.
- (16) Yamazaki, I.; Akimoto, S.; Yamazaki, T.; Sato, S.-I.; Sakata, Y. Oscillatory Exciton Transfer in Dithiaanthracenophane: Quantum Beat a Coherent Photochemical Process in Solution. *J. Phys. Chem. A* **2002**, *106*, 2122–2128.
- (17) Zhu, F.; Galli, C.; Hochstrasser, R. M. The Real-Time Intramolecular Electronic Excitation Transfer Dynamics of 9',9-Bifluorene and 2',2-Binaphthyl in Solution. *J. Chem. Phys.* **1993**, *98*, 1042–1057.
- (18) Sato, S.-I.; Nishimura, Y.; Sakata, Y.; Yamazaki, I. Coherent Control of Oscillatory Exciton Transfer in Dithia-1,5(3,3)-anthracenophane by a Phase-Locked Femtosecond Pulse Pair. *J. Phys. Chem. A* **2003**, *107*, 10019–10025.
- (19) Kato, T.; Fujimura, Y. Intermolecular Interaction-Induced Quantum Beats in Femtosecond Time-Resolved Light Scattering from Molecules: Photon-Polarization and Inhomogeneous Effects. *Chem. Phys.* **1996**, *202*, 95–106.
- (20) Yang, L.; Caprasecca, S.; Mennucci, B.; Jang, S. Theoretical Investigation of the Mechanism and Dynamics of Intramolecular Coherent Resonance Energy Transfer in Soft Molecules: A Case Study of Dithia-anthracenophane. *J. Am. Chem. Soc.* **2010**, *132*, 16911–16921.
- (21) Tretiak, S.; Chernyak, V.; Mukamel, S. Two-Dimensional Real-Space Analysis of Optical Excitations in Acceptor-Substituted Carotenoids. *J. Am. Chem. Soc.* **1997**, *119*, 11408–11419.
- (22) Tretiak, S.; Chernyak, V.; Mukamel, S. Collective Electronic Oscillators for Nonlinear Optical Response of Conjugated Molecules. *Chem. Phys. Lett.* **1996**, *259*, 55–61.
- (23) Stewart, J. J. P. Optimization of Parameters for Semiempirical Methods 0.1. *Method. J. Comput. Chem.* **1989**, *10*, 209–220.
- (24) Stewart, J. J. P. Optimization of Parameters for Semiempirical Methods. II. Applications. *J. Comput. Chem.* **1989**, *10*, 221–264.
- (25) Thouless, D. J. *The Quantum Mechanics Of Many-Body Systems*; Academic Press: New York, 1972.
- (26) Davidson, E. R. *Reduced Density Matrices in Quantum Chemistry*; Academic Press: New York, 1976.
- (27) Hirata, S.; Head-Gordon, M.; Bartlett, R. J. Configuration Interaction Singles, Time-Dependent Hartree-Fock, and Time-Dependent Density Functional Theory for the Electronic Excited States of Extended Systems. *J. Chem. Phys.* **1999**, *111*, 10774–10786.
- (28) Bazan, G. C.; Oldham, W. J.; Lachicotte, R. J.; Tretiak, S.; Chernyak, V.; Mukamel, S. Stilbenoid Dimers: Dissection of a Paracyclophane Chromophore. *J. Am. Chem. Soc.* **1998**, *120*, 9188–9204.
- (29) Tretiak, S.; Chernyak, V.; Mukamel, S. Excited Electronic States of Carotenoids: Time-Dependent Density-Matrix-Response Algorithm. *Int. J. Quantum Chem.* **1998**, *70*, 711–727.
- (30) Tretiak, S.; Chernyak, V.; Mukamel, S. Chemical Bonding and Size Scaling of Nonlinear Polarizabilities of Conjugated Polymers. *Phys. Rev. Lett.* **1996**, *77*, 4656–4659.
- (31) Tretiak, S.; Chernyak, V.; Mukamel, S. Localized Electronic Excitations in Phenylacetylene Dendrimers. *J. Phys. Chem. B* **1998**, *102*, 3310–3315.
- (32) Dreuw, A.; Head-Gordon, M. Single-Reference Ab Initio Methods for the Calculation of Excited States of Large Molecules. *Chem. Rev.* **2005**, *105*, 4009–4037.
- (33) Tully, J. Molecular Dynamics with Electronic Transitions. *J. Chem. Phys.* **1990**, *93*, 1061–1071.
- (34) Hammes-Schiffer, S.; Tully, J. C. Proton-Transfer in Solution: Molecular-Dynamics with Quantum Transitions. *J. Chem. Phys.* **1994**, *101*, 4657–4667.
- (35) Paterlini, M.; Ferguson, D. Constant Temperature Simulations using the Langevin Equation with Velocity Verlet Integration. *Chem. Phys.* **1998**, *236*, 243–252.
- (36) Attard, P. Statistical Mechanical Theory for Non-Equilibrium Systems. IX. Stochastic Molecular Dynamics. *J. Chem. Phys.* **2009**, *130*, 194113.
- (37) Tretiak, S.; Isborn, C.; Niklasson, A.; Challacombe, M. Representation Independent Algorithms for Molecular Response Calculations in Time-Dependent Self-Consistent Field Theories. *J. Chem. Phys.* **2009**, *130*, 054111.
- (38) Tretiak, S.; Chernyak, V.; Mukamel, S. Recursive Density-Matrix-Spectral-Moment Algorithm for Molecular Nonlinear Polarizabilities. *J. Chem. Phys.* **1996**, *105*, 8914–8928.
- (39) Furche, F.; Ahlrichs, R. Adiabatic Time-Dependent Density Functional Methods for Excited State Properties. *J. Chem. Phys.* **2002**, *117*, 7433–7447.
- (40) Nelson, T.; Fernandez-Alberti, S.; Chernyak, V.; Roitberg, A. E.; Tretiak, S. Nonadiabatic Excited-State Molecular Dynamics Modeling of Photoinduced Dynamics in Conjugated Molecules. *J. Phys. Chem. B* **2011**, *115*, 5402–5414.
- (41) Send, R.; Furche, F. First-Order Nonadiabatic Couplings from Time-Dependent Hybrid Density Functional Response Theory: Consistent Formalism, Implementation, and Performance. *J. Chem. Phys.* **2010**, *132*, 044107.
- (42) Tavernelli, I.; Curchod, B. F. E.; Laktionov, A.; Rothlisberger, U. Nonadiabatic Coupling Vectors for Excited States within Time-Dependent Density Functional Theory in the Tamm-Dancoff Approximation and Beyond. *J. Chem. Phys.* **2010**, *133*, 194104.
- (43) Nelson, T.; Fernandez-Alberti, S.; Chernyak, V.; Roitberg, A.; Tretiak, S. Nonadiabatic Excited-State Molecular Dynamics: Numerical Tests of Convergence and Parameters. *J. Chem. Phys.* **2012**, *136*, 054108.
- (44) Fernandez-Alberti, S.; Roitberg, A.; Nelson, T.; Tretiak, S. Identification of Unavoided Crossings in Nonadiabatic Photoexcited Dynamics Involving Multiple Electronic States in Polyatomic Conjugated Molecules. *J. Chem. Phys.* **2012**, *137*, 014512.
- (45) Nelson, T.; Fernandez-Alberti, S.; Roitberg, A. E.; Tretiak, S. Artifacts Due to Trivial Unavoided Crossings in the Modeling of Photoinduced Energy Transfer Dynamics in Extended Conjugated Molecules. *Chem. Phys. Lett.* **2013**, *590*, 208–213.
- (46) Nelson, T.; Fernandez-Alberti, S.; Roitberg, A. E.; Tretiak, S. Nonadiabatic Excited-State Molecular Dynamics: Treatment of Electronic Decoherence. *J. Chem. Phys.* **2013**, *138*, 224111.
- (47) Nelson, T.; Fernandez-Alberti, S.; Roitberg, A. E.; Tretiak, S. Nonadiabatic Excited-State Molecular Dynamics: Modeling Photo-physics in Organic Conjugated Materials. *Acc. Chem. Res.* **2014**, *47*, 1155–1164.
- (48) Tretiak, S.; Mukamel, S. Density Matrix Analysis and Simulation of Electronic Excitations in Conjugated and Aggregated Molecules. *Chem. Rev.* **2002**, *102*, 3171–3212.
- (49) Wu, C.; Malinin, S. V.; Tretiak, S.; Chernyak, V. Y. Multiscale Modeling of Electronic Excitations in Branched Conjugated Molecules using an Exciton Scattering Approach. *Phys. Rev. Lett.* **2008**, *100*, 057405.

(50) Beljonne, D.; Yamagata, H.; Bredas, J. L.; Spano, F. C.; Olivier, Y. Charge-Transfer Excitations Steer the Davydov Splitting and Mediate Singlet Exciton Fission in Pentacene. *Phys. Rev. Lett.* **2013**, *110*, 226402.

(51) Silbey, R.; Hortner, J.; Rice, S. A. On the Singlet-Exciton States of Crystalline Anthracene. *J. Chem. Phys.* **1965**, *42*, 1515–1534.

(52) Kurik, M. V.; Piryatinskii, Y. P.; Popel, O. M.; Frolova, E. K. Temperature Dependence of the Davydov Splitting in Anthracene. *Phys. Status Solidi* **1970**, *37*, 803–806.

(53) Szabo, A. Theory of Fluorescence Depolarization in Macromolecules and Membranes. *J. Chem. Phys.* **1984**, *81*, 150–167.

(54) Lakowicz, J. *Principles of Fluorescence Spectroscopy*; Springer Verlag: New York, 2006.